PROGRESS IN COLOR, COLORANTS AND COATINGS

available online @ www.pccc.icrc.ac.ir

Prog. Color Colorants Coat. 12 (2019), 1-14

Ministry of Science, Research and Technology
Institute for Color Science and Technology

Control over Power Conversion Efficiency of BHJ Solar Cells: Learn more from Less, with Artificial Intelligence

A. Ashtiani Abdi[1], F. Nourmohammadian[1,2*], Y. Mohammadi[3], M. R. Saeb[4]

[1.] Department of Organic Colorants, Institute for Color Science and Technology, P.O. Box 16765-654, Tehran, Iran
[2.] Center of Excellence for Color Science and Technology, Institute for Color Science and Technology, P.O. Box 16765-654, Tehran, Iran
[3] Petrochemical Research and Technology Company (NPC-rt), National Petrochemical Company (NPC), Tehran, Iran
[4.] Department of Resin and Additives, Institute for Color Science and Technology, P.O. Box: 16765-654, Tehran, Iran

ARTICLE INFO

Article history:
Received: 28 Oct 2018
Final Revised: 16 Dec 2018
Accepted: 17 Dec 2018
Available online: 13 Jan 2019

Keywords:
Bulk heterojunction solar cells
Artificial neural network
Genetic algorithm
Multi-objective optimization.

ABSTRACT

Harvesting the energy from the sun through the bulk heterojunction (BHJ) solar cells need materials with specific electronic characteristics. However, any promising material if cast improperly in cells will end into low or even null power conversion efficiency (PCE). Cell casting optimization is a time/material consumable step in any photovoltaic manufacturing practice. In this study, we showed that how the artificial intelligence (AI) could help to find optimum values of device preparation variables. For this purpose, an in-house code will catch the input variables (donor: acceptor ratio, spin casting rate, annealing temperature); learn the trends by the hybrid artificial neural network (ANN), genetic algorithm (GA) and optimize the output results simultaneously. The results showed that ANN/GA is capable to learn the trends of relatively small size dataset without over-fitting. This study highlights that how implementing the suggested AI model can help to learn more information and find the optimum recipe from less number of experiments with the highest precision. Prog. Color Colorants Coat. 12 (2019), 1-14© Institute for Color Science and Technology.

1. Introduction

Harvesting energy from renewable sources has become an important topic in the last few decades following escalating environmental concerns [1]. Meanwhile, emerging of organic solar cells (OSC) has caught eyes of researchers and industry hopping to find a solution for low cost and bulk production of solar cells [2]. Very recently, a generation of OSCs known as bulk heterojunction (BHJ) solar cells showed specific desirable characteristics like lightweight, flexibility, print or role-to-role application and low-cost production in addition to promising efficiency [3, 4]. Just like any solar cell technology, BHJ architecture consists of several stacked layers with different roles in the mechanism of converting energy from solar radiation to electricity. However, the active layer of BHJ composes of an inhomogeneous mixture of at least two organic materials that absorb photons, produce electron-hole pairs (exciton), dissociate it to charge carriers and conduct the carries to be finally collected at the electrodes [5]. It is important to construct an active layer with nano-scale morphology in accordance with the lifetime of excitons. Knowing the fact that there is no perceptible instruction to

*Corresponding author: nour@icrc.ac.ir

control this morphology, the experimental optimization of the cells became an extensive time and material-consuming step in any BHJ investigation [6, 7].

Therefore, the heterogeneous nature of the active layer adds more complexity in BHJ compared with other types of solar cells. Nevertheless, when it comes to complexity, the artificial intelligence (AI) is definitely the best solution to deal with the problem. Despite the recent developments in integration of AI in the field of organic electronics, they mainly emphasize on the design aspects of organic molecules [8-13] and far too little attention has been paid to address the device considerations [14].

The present paper aims to investigate the capability of AI for learning the trend of working parameters of solar cells (J, V, FF, PCE) as the output of the model by changing the cell casting variables (input) from a limited number of experimental data points. After solving the problem of model overfitting on relatively small datasets, it will be possible to ask the model for adjusting the variables to find the best possible cell performance and deliver the clear understandings of the individual influence of each changing variables on the resulting parameters.

To seek for addressing the mentioned question, we developed an in-house artificial neural network (ANN) code with genetic algorithm (GA) for multi-objective optimization of inputs. A dataset of experimental data of BHJ cells was picked with three essential casting parameters; donor to acceptor ratio, thermal annealing temperature and spin rate of spin coater. The aspects of the model, further discussions about the successful modeling of the data and clarifying the relationships between distinct input-output are also dealt with in more detail in next sections.

2. Model Development

2.1. Individual optimization

Modeling with ANN involves training and test procedures, whereby weights and thresholds (biases) will be systematically manipulated to minimize the prediction error. Accordingly, the developed network learns the behavior of the process. The error occurring during the network configuration can be controlled by adaptation of a set of data as the training datasets for the network. Then, the outputs will be controlled and tuned by the model comparing the actual (target) experimental values with those proposed by the model until reaching the desired minimum error. Upon completion of training, the educated ANN enables prediction of the rest of the dataset.

A dataset of 27 data points (scenario) is picked for training the model [15]. The Inputs are annealing temperature (x_1), the donor ($BT(TDPP_{EH}TTT_{C6})_2$) to acceptor (PC71BM) ratio, which is changed to donor content (x_2), and the rotation rate of spin coater (x_3), each in 3 levels. The outputs are short-circuit current density, $J_{sc,}$ (y_1), open circuit voltage, V_{oc}(y_2), fill factor, FF (y_3), and power conversion efficiency; PCE (y_4). The donor component of the active layer in BHJ devices is of a DPP backbone that is similar to the DPP-BT structures which we designed recently [16].

To construct ANN models for predicting y_1 to y_4, the data were randomly separated into two sets. In one set, nineteen scenarios were selected out of overall twenty-seven scenarios to train the network, and in the other set, the remaining eight scenarios were used to test the reliability of each ANN. This process was repeated until the desired degree of error was achieved.

There are some difficulties associated with choosing the ANN architecture; hence, the number of layers and neurons of each one for a given problem should be selected cautiously. Nonetheless, the complexity of the problem is a function of the extent to which the programmer is acquainted with the nature of the manufacturing process.

Basically, there is no standard for choosing and implementing the architecture for ANN, and the number of layers and neurons for a problem depends on the difference between the number of input and output variables [17, 18]. In general, the nature of the manufacturing process is not known, but for such complex systems, the professional developed computer code, instead of using simplified versions of ANN or GAs as software packages, can learn it as far as possible [19].

The ANN models were trained individually by feeding the first random set of data in each case, which were not essentially the same. Then, the biases and weights of interconnections among the neurons were manipulated by the code until reaching the desired error level. The ANNs were then tested against the remaining data, i.e. test dataset. The activating function in this study is a hyperbolic tangent sigmoid (Eq. 1).

$$f(x) = \frac{e^{x}-e^{-x}}{e^{x}+e^{-x}} \quad (1)$$

Implementing GA brings the optimization capability to the model. The weights and biases of the ANN model act as chromosomes of the GA optimizer. The structure of the defined chromosome is illustrated in Figure 1. Unknown parameters of the network were 291 coded as a chromosome composed of 291 components or genes. The initial 246 genes in this chromosome are representative of the unknown weights of the ANN, while the remaining of 45 genes are those dedicated to the unknown biases, which are placed correspondingly one after another from left to right in the defined chromosome.

To optimize parameters of the model, a population of 50 chromosomes is randomly generated and the information of each chromosome, e.g. chromosome number *j*, is independently situated into the predefined ANN structure. The network in each case was evaluated with respect to the weights and biases dictated by the assigned chromosome.

The validity of the model was confirmed by assessing the predicted values proposed by ANN through statistical criteria defined in Eq. 2 and 3:

$$MSE = \frac{1}{N}\sum_{i=1}^{N}(y_{i,predicted} - y_{i,target})^2 \quad (2)$$

$$Error = \frac{\sqrt{MSE}}{Max(Error)} \times 100 \quad (3)$$

where *MSE* is the mean of the squared error and $y_{i,predicted}$ and $y_{i,target}$ are the output of the model and the experimental target, respectively. Moreover, N is representative of the number of data used for training, and *Max* (*Error*) is the maximum network error. To minimize the *MSE*, the chromosomes were sorted considering their *MSE*s. Then, selection, mating, crossover, and mutation operators were applied to the population and the optimization process continued until the desired chromosome was obtained. The mating operator couples the rest of the chromosomes as dictated by the roulette wheel selection mechanism [20]. The mating operator was put into the creation of child chromosomes after parent chromosomes experienced crossover. In the next step, the mutation operator randomly selected one gene out of the gene pool and exchanged its value stochastically. The flowchart of the modeling process is shown in Figure 2. In the current section, single-objective optimization part of our code is described. The multi-objective optimization illustrated in the sketch will be explained in the following section.

We used Lazarus IDE and FPC 2.6.2 packages for programming and compiling the in-house ANN/GA code running on windows 7 operating system with Intel Core i7-3770K (3.50 GHz) processor and 32 GB of memory (2133 MHz).

2.2. Multi-objective optimization

In the previous section, individual optimization of each response was carried out leading to the construction of four optimized ANN models. In a practical case, it is essential to identify the best input levels aimed at reaching the optimum values of the outputs at the same time.

In general, Non-dominated Sorting Genetic Algorithm-II (NSGA-II) [21-23] determines the optimum values of the variables and encodes them so that each chromosome has n genes proportional to the number of input variables. As previously noted, inputs include 3 parameters, which are annealing temperature, donor content, and spin rate. GA algorithm simultaneously adjusts J_{sc}, V_{oc}, and FF criteria.

The initial population of the mentioned chromosomes is produced to initiate the process of genetic evolution algorithm optimization method. For the production of chromosomes, the value for each gene is randomly selected. Following the generation of the initial population, it is required to measure goodness-of-fit value for each chromosome as it represents a recipe scenario to produce a BHJ module. It is definitely apparent that maximizing all the 3 outputs would be the desirable target to reach the utmost PCE value.

Figure 1: Structures of defined chromosomes.

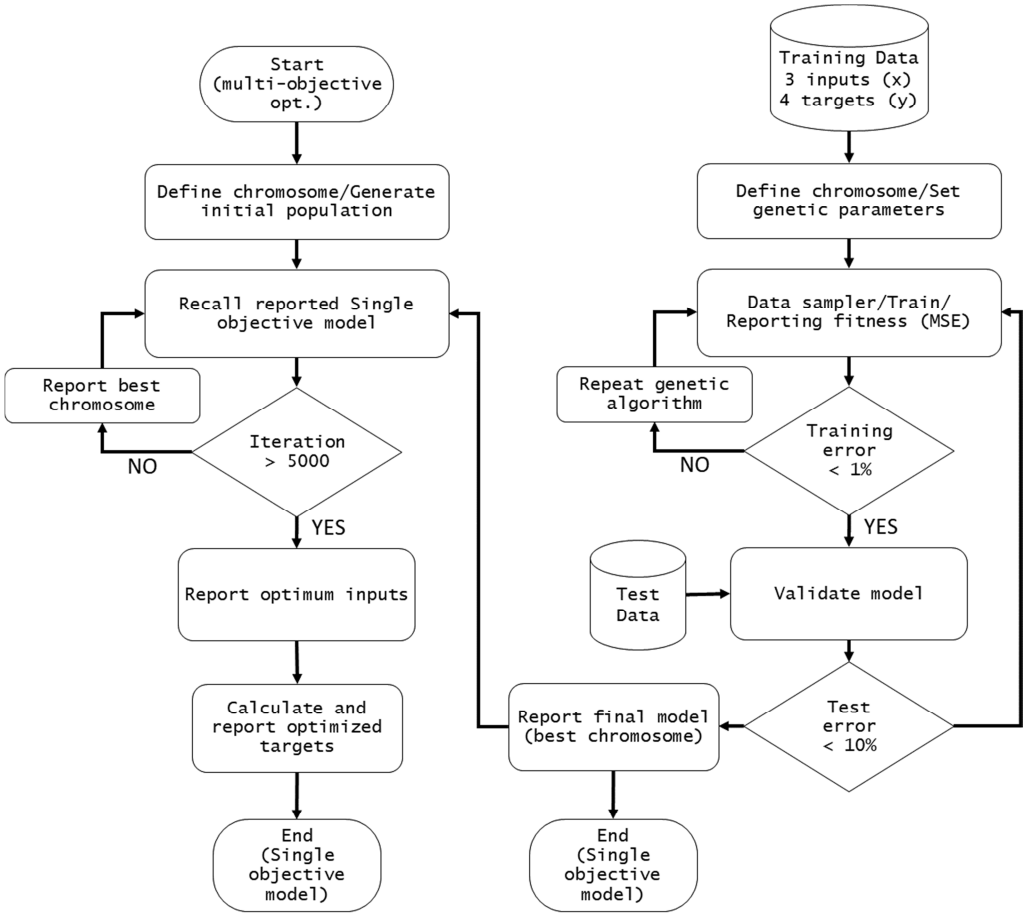

Figure 2: Flowchart of single and multi-objective ANN/GA hybrid model.

To determine the fitness of any selected chromosome and to properly sort the chromosomes from favorable to unfavorable, the non-dominated sorting genetic algorithm was applied. Accordingly, it is crucial to arrange the rank and quality of chromosomes. The quality is a primary criterion due to its remarkable significance in sorting chromosomes. By considering this criterion, all chromosomes are mutually compared with each other while the dominated one attains a negative rating.

Any given chromosome *i* prevails the chromosome *j*, if its value is one unit higher or equal to chromosome *j*.

In order to calculate each of the objective functions, a neural network associated with the function being created in the first phase can be employed. That is, for each chromosome, all final optimal ANNs are recalled individually. Moreover, the outputs that are target functions for chromosome *I* are calculated per inputs which are the same genes of chromosome *i*.

After comparing each pair of chromosomes, the chromosomes not predominated even once are isolated from the rest of the chromosomes and classified as the first Pareto front [24]. This procedure is repeated for other chromosomes to determine Pareto fronts 2, 3, etc. Obviously, Pareto front number *n* is related to the chromosomes that have been beaten (*n*-1) times. Afterward, a secondary criterion, which refers to the crowding distance of chromosomes in each Pareto front, can be used for sorting. To address this, after arranging each objective, the errors in the prediction of each response were specified and the multi-objective optimization was validated based on achieving the minimum value of the overall error, i.e. the sum of errors in the prediction of each response when they are adjusted simultaneously [25].

After calculating the degree of fitness based on the primary and secondary criteria, entire chromosomes are

sorted from the most favorable to the least favorable ones. Apparently, the best chromosomes are related to the first Pareto front, which have the least amount of the target functions. Accordingly, selecting, pairing, reproducing and mutating are carried out and parents as well as children of the new generation are taken to re-evaluate the fitness, again based on the non-dominated sorting algorithm. In Table 1, the values of various parameters used in the BHJ cell functions optimization with evolutionary algorithm NSGA-II are listed.

The condition for the completion of optimization process is set at 20,000 iterates. The module of multi-objective optimization has been already provided in Figure 2. This module contains an efficient computer code, which is able to recall optimal ANNs trained in the first phase of modeling and implements the GAs algorithm based on multi-objective optimization process.

3. Results and Discussion

3.1. Modeling the BHJ functions by GA-based ANN approach

As noted in the previous section, the model will seek among the training-test dataset combinations to reach the lowest *MSE* error during the training phase. Figure 3 shows the variation of *MSE*s related to the best arrangement (chromosome) in the training phase of the network. On the basis of the admitted number of epochs and very low final error, the behavior of outputs with regard to the selected inputs are satisfactorily predictable by the model.

Table 1: The second phase of the algorithm parameters to optimize multi-objective evolutionary genetics.

Optimization Parameter	Value
Initial population size	100
Selection Mechanism	Ternary Tournament Selection
Mating Mechanism	Roulette wheel selection
Crossover Mechanism	Single-point crossover
Mutation rate	15%

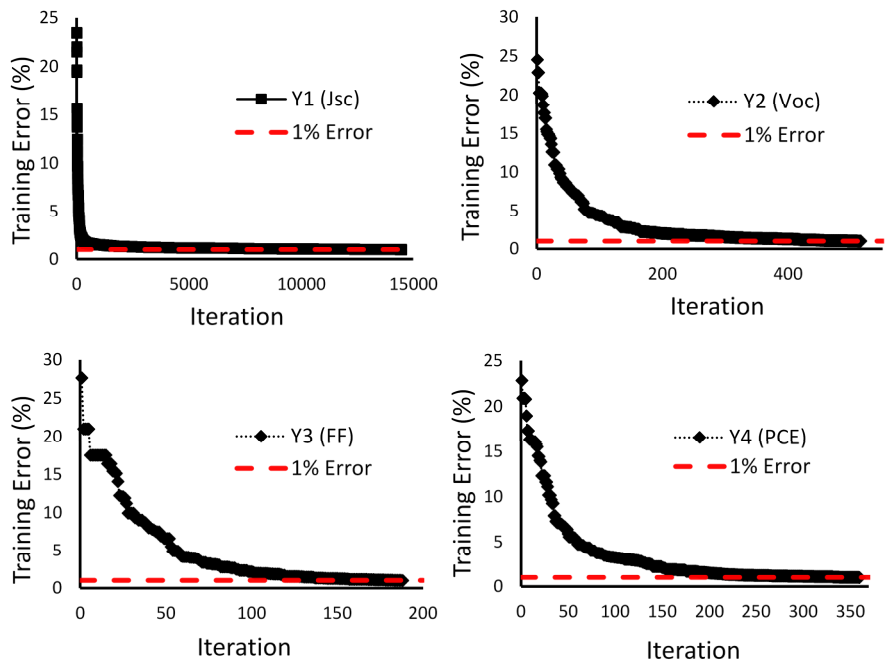

Figure 3: Training error of the responding variables (y) which reaches to 1% during ANN model optimization iterations.

By comparing the predicted and target values of each response, the performance of the ANN can be further examined. Figure 4 compares the experimental and model values. The plots put stress on the fact that the ANNs developed for each prediction of each response appropriately match with the experimental pattern. The results in Figure 4 show that the ANN can predict the experimental target values at high acceptable accuracy.

The precision of the network which is trained by the experimental data is illustrated from another standpoint in Figure 5. The vicinity of data point to the ideal y=x line suggests an accurate prediction model which is rooted in the synergic effect of both ANN and GA.

3.2. Visualization the particular impact of inputs on the responses

A number of studies have been made to reflect the impact of cell manufacturing parameters on the cell functions in the fashion of mathematical elucidation [26-34]. Herein, to demonstrate the complex and, somehow, controversial nature of such an important issue, the capabilities of artificial intelligence are investigated. To address this objective, the model outputs are treated and interpreted in this section.

Figure 6 shows the behavior of J_{sc} (y_1) predicted by the model versus three input variables. Subplot-A demonstrates J_{sc} values between 1.2 to 2.2 $mA.cm^{-2}$ by color and size in a three-dimensional space of donor content (0.3 to 0.7), spin rate (1000 to 4000 rpm) and annealing temperature (as-cast in room temperature to 110 °C). The bigger balls are representative of recipes, which will result in higher J_{sc}. This plot illustrates that the annealing has an improper effect on the J_{sc}. Then, the best condition to get higher J_{sc} values will be achieved by the donor to acceptor ratios around 40:60 (donor content 0.4), mild film casting rate of 2000 rpm and employing the cell as cast.

To examine the effect of each individual input on the J_{sc}, it is useful to draw the surfaces of output by two of the inputs at a specific value of the third input. Figure 6-B demonstrates the effect of donor content and spin coating rate on J_{sc} of an as-cast active layer. The plot shows that while the donor content has a dominant effect on J_{sc}, the casting spin rate has a minor effect on increasing the J_{sc}.

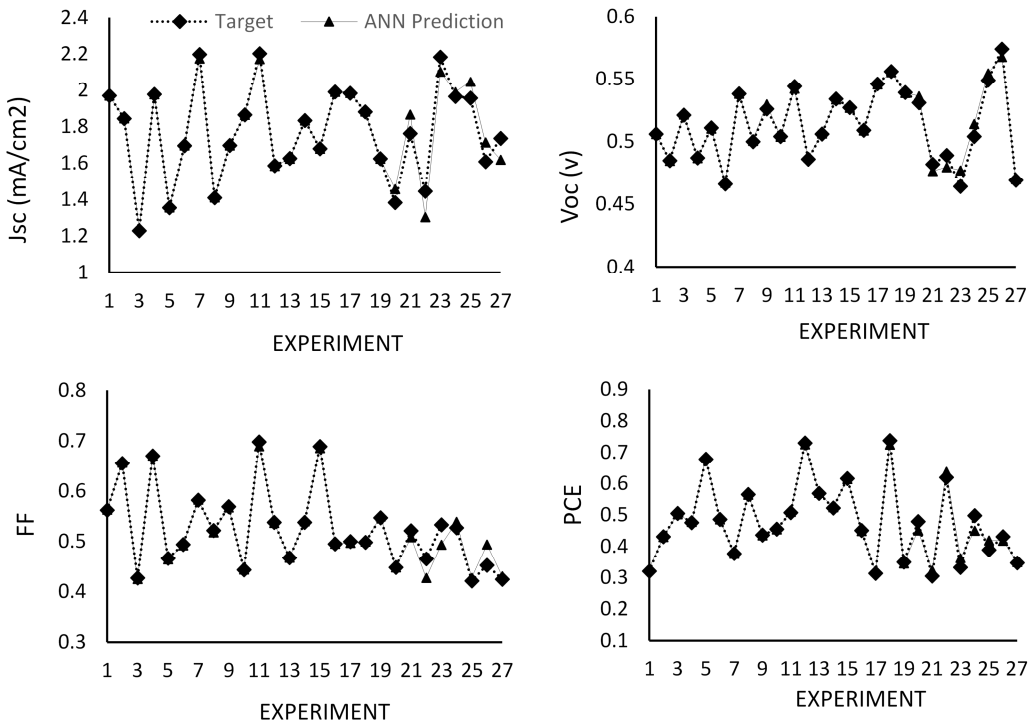

Figure 4: Experimental targets versus ANN prediction values.

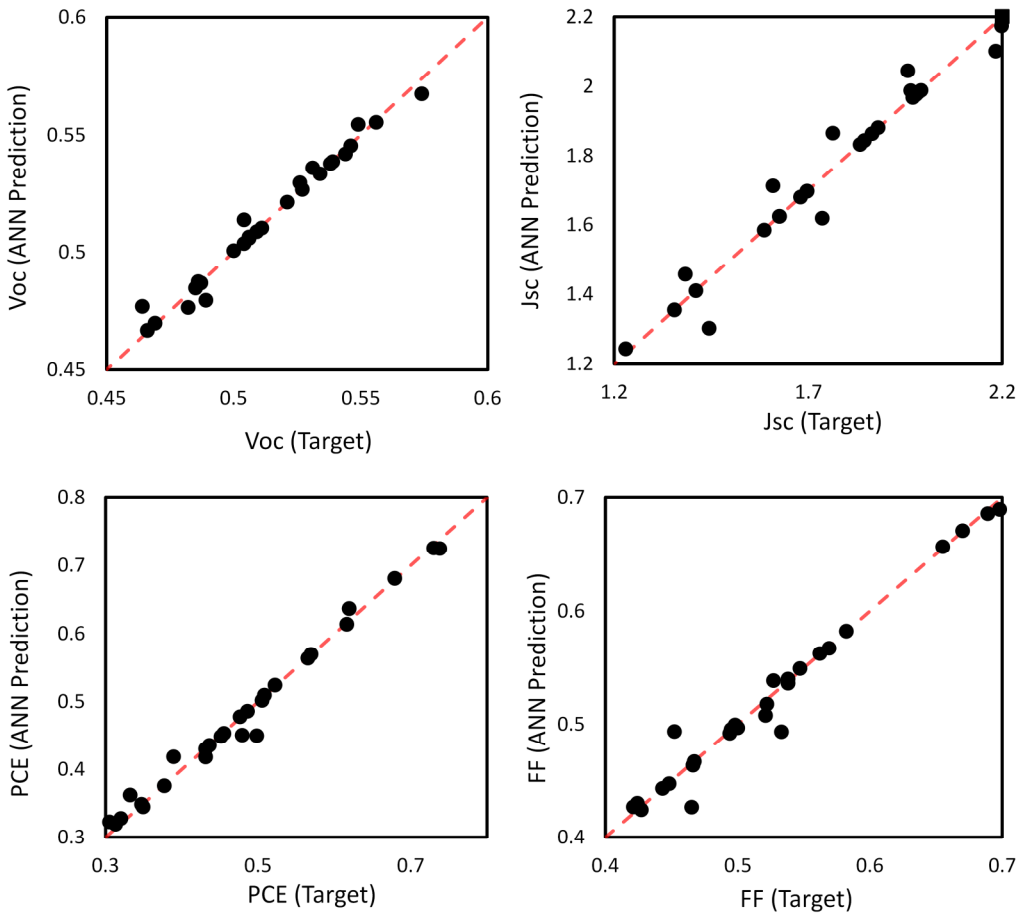

Figure 5: Comparison of the experimental data and the ANN model outputs.

According to Figure 6-C, when the J_{sc} is plotted versus donor content and annealing temperature at the spin rate of 2000 rpm, the same limited effect of annealing temperature on J_{sc} as that of the spin rate can be seen. According to both B and C plots in Figure 6, the J_{sc} of a cell falls dramatically when the donor share is more than acceptor (higher than 0.5). In other words, J_{sc} has influenced mainly by donor content than the annealing while the spin rate is 2000 rpm or casting speed variation of an un-annealed film. At higher donor ratios, e.g. 70:30, the J_{sc} is more sensitive to the film casting rate and annealing, in such a way that increasing both of the inputs will deteriorate J_{sc} (Figure 6-D).

However, once choosing the optimum donor content as shown in Figure 6-E, the level of J_{sc} is generally high and further improvements can be achieved by the vicinity the spin rate in the vicinity of 2000 rpm. This observation suggests that for the chosen donor and acceptor compounds, optimizing the donor to acceptor ratio, independent of annealing or the rate of the film casting condition, is at the highest degree of importance.

Unlike the J_{sc}, fill factor is highly influenced by physical film-forming parameters, annealing temperature, and spin coating rate as well as donor content. Both the plots B and C in Figure 7 show similar sensitive reductive trends by increasing temperature and spin rate. For both the mentioned situations, the optimum D/A range to reach a high FF is narrow the same for J_{sc}. Consequently, the domain of high-FF zone is not noticeably broad due to its sensitivity to more parameters. Specifically, there is no need for annealing or increasing the spin rate.

The value of J_{sc} relates to the number of photons absorbed within the active layer, hence it can be suppressed by imperfect charge separation and charge collection. FF is determined by the competition between the photo-generation and recombination of charge carriers to the ground state [26]. As expected, our modeling demonstrates that both J_{sc} and FF are directly governed by the quality of nanoscale heterojunction net construction of active layer [35, 36].

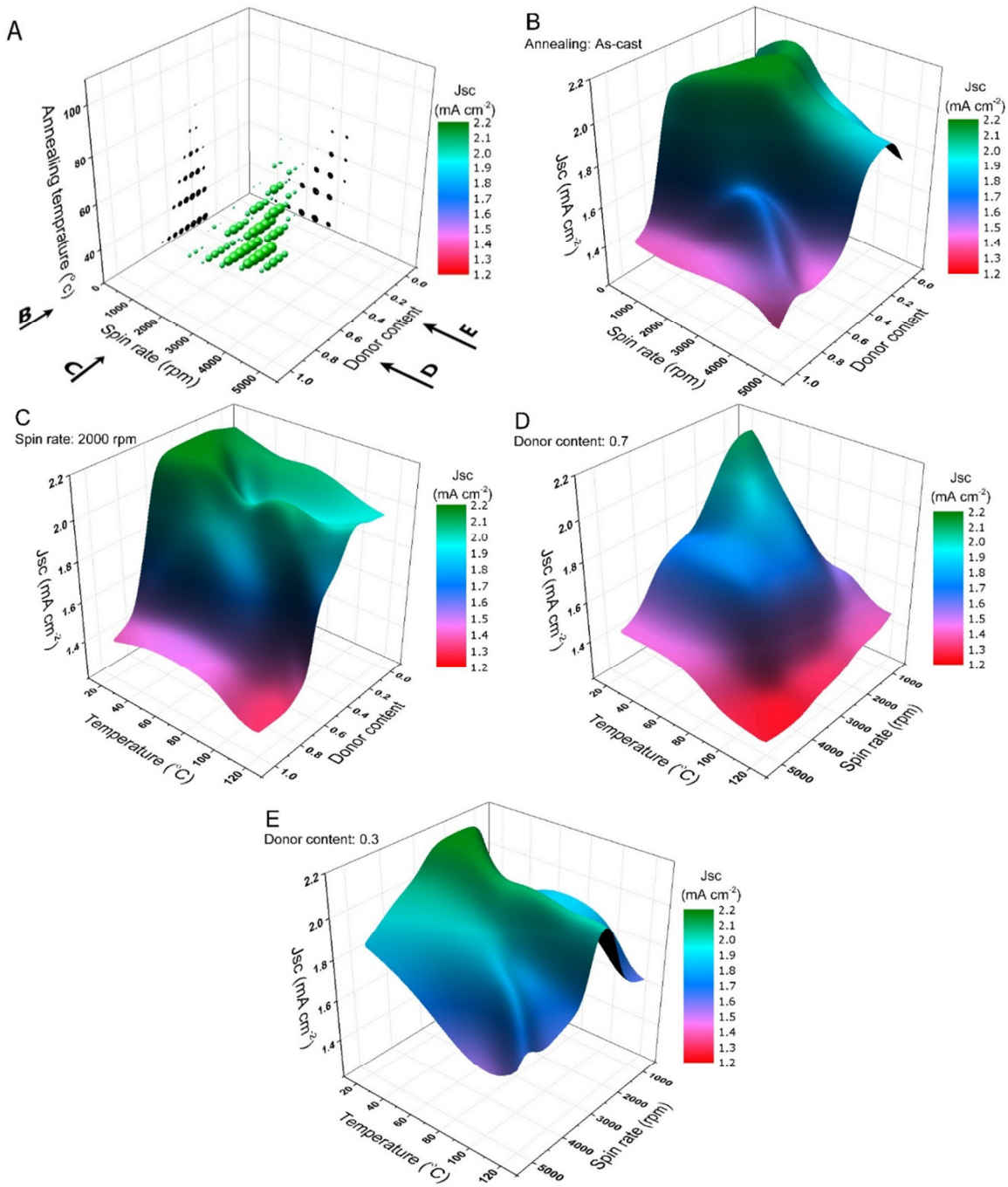

Figure 6: Three-dimensional plots predicted from the ANN model representing the effect of donor content, annealing and spin rate of film casting on J_{sc}.

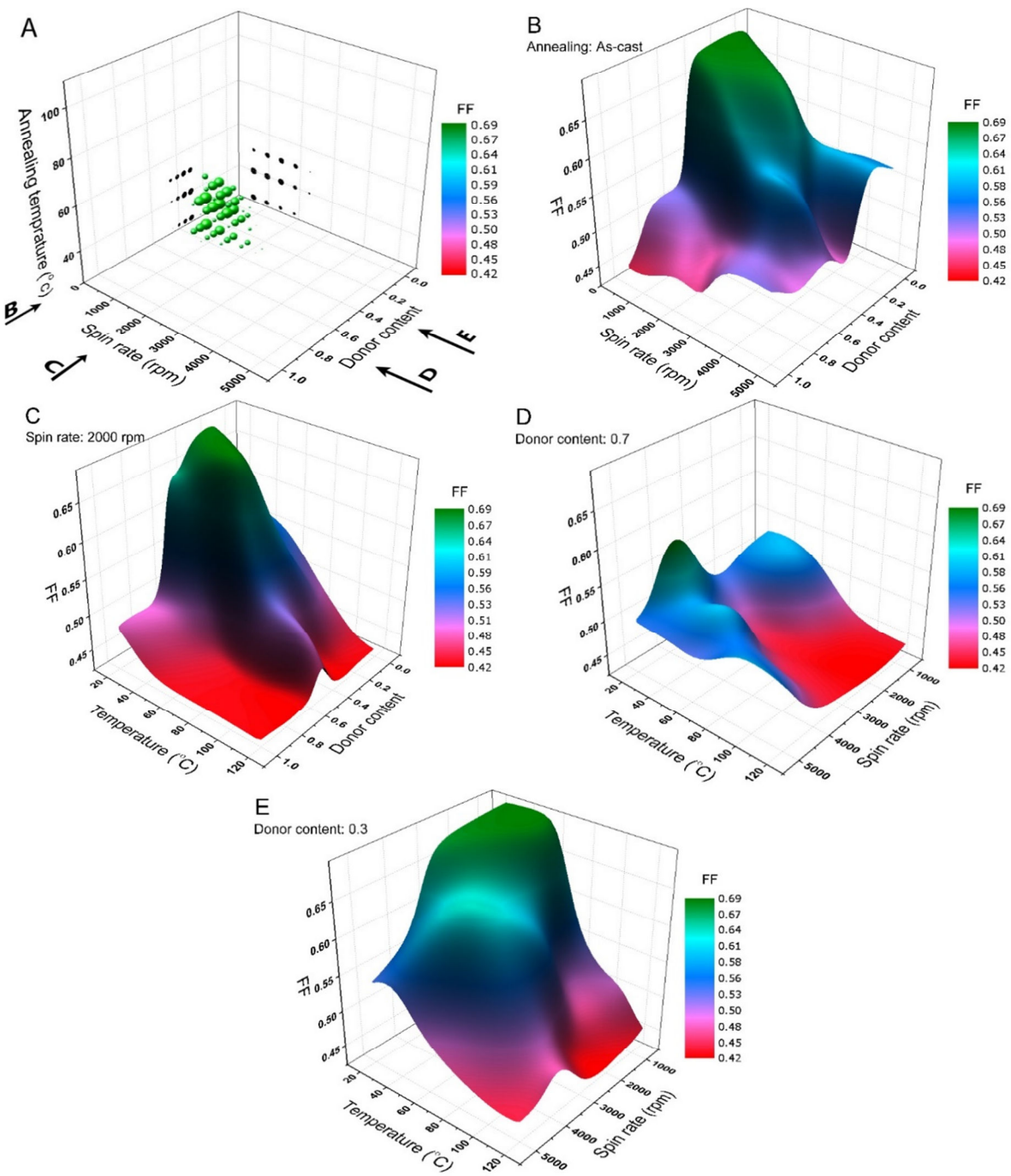

Figure 7: Three-dimensional plots predicted from the ANN model representing the effect of donor content, annealing and spin rate of film casting on FF.

The trend of input parameter variations on the V_{oc} is shown in. Compared with J_{sc} and FF, the surfaces of V_{oc} change wavy and without meaningful trend. The non-smooth dependent functionality of V_{oc} of physical film formation parameters and composition of the active layer is to some extent a proof for the claim that V_{oc} mainly depends on the intrinsic molecular energy levels of donor and its acceptor counterpart [37, 38]. Anyway, independent behavior does not mean the absence of any relation. It is reported that donor content, and so the extent of interfacial area between specific donor-acceptor mixture, will alter the V_{oc} value [39], Figure 8, B and C reveals the similar picture too. According to Figure 8, D, V_{oc} is rising with temperature. The same trend is slightly observed for higher spin rates. Hence, according to the results, the model depicts that more studies are needed in connection with film casting conditions, especially

annealing condition and film casting rate V_{oc}.

Theoretically, V_{oc} is considered to be correlated with the energy gap between the HOMO of the donor and the LUMO of the acceptor in BHJ structure with a margin of different kinds of losses [38]. Then, it is common to confine the V_{oc} in a chemical vale with some assumptions which may suggest simplifications of theories [37]. However, illustrations in this study support the findings in a number of reports about the dependency of V_{oc} on different casting conditions like temperature, light intensity, nano-morphology, the balance between charge separation and recombination, the energy of emissive charge-transfer (CT) states, and energetic disorder [40, 41].

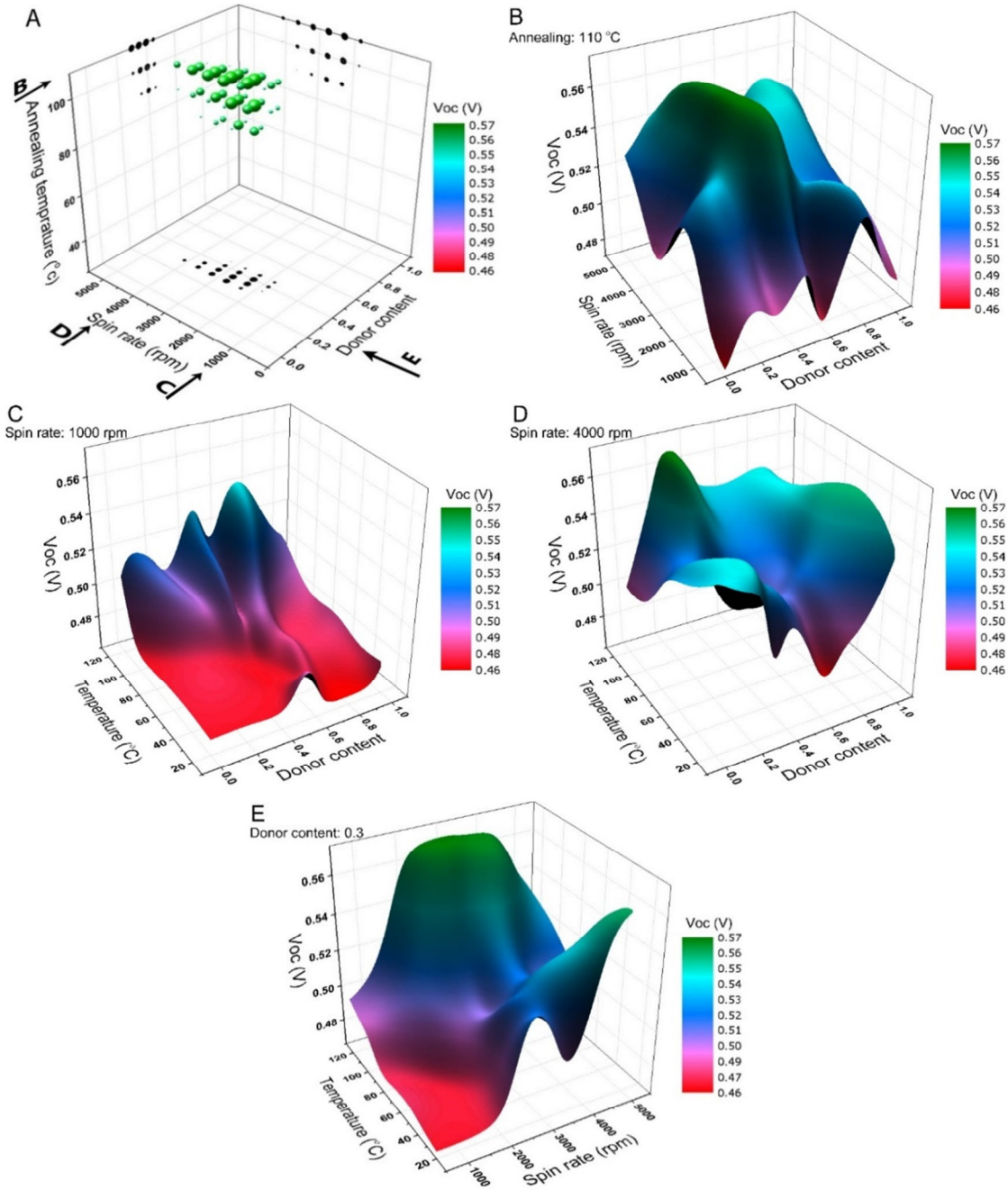

Figure 8: Three-dimensional plots predicted from the ANN model representing the effect of Donor content, annealing and spin rate on V_{oc}.

The last sets of illustration highlighted the true behavior of working parameters of the PV system (J_{sc}, $V_{oc,}$ and FF) against variation of the individual input parameter. However, they showed that gaining J_{sc} and FF means a reduction in V_{oc}. Therefor, it is not possible to directly deduce the best recipe for highest PCE. Figure 9 demonstrates the result of the last output (PCE) optimization. Comparing the first sub-figures in Figure 9 and Figure 6 shows that the suggested regions for maximizing PCE and J_{sc} are identical. Figure 9-B to 9-E are also consistent with the respective sub-figures in Figure 6. This means a strong synergistic governing effect of J_{sc} and FF (Figure 7-A) on the final efficiency.

The visually derived aforementioned results closely match those obtained by multi-objective modeling. The proposed ANN/GA multi-criteria optimization with the dictated criteria for maximizing all the three outputs (J_{sc}, $V_{oc,}$ and FF) delivers the PCE 0.76 for optimum donor content of 0.45, the annealing temperature of 41 °C and spin rate of 2403 rpm.

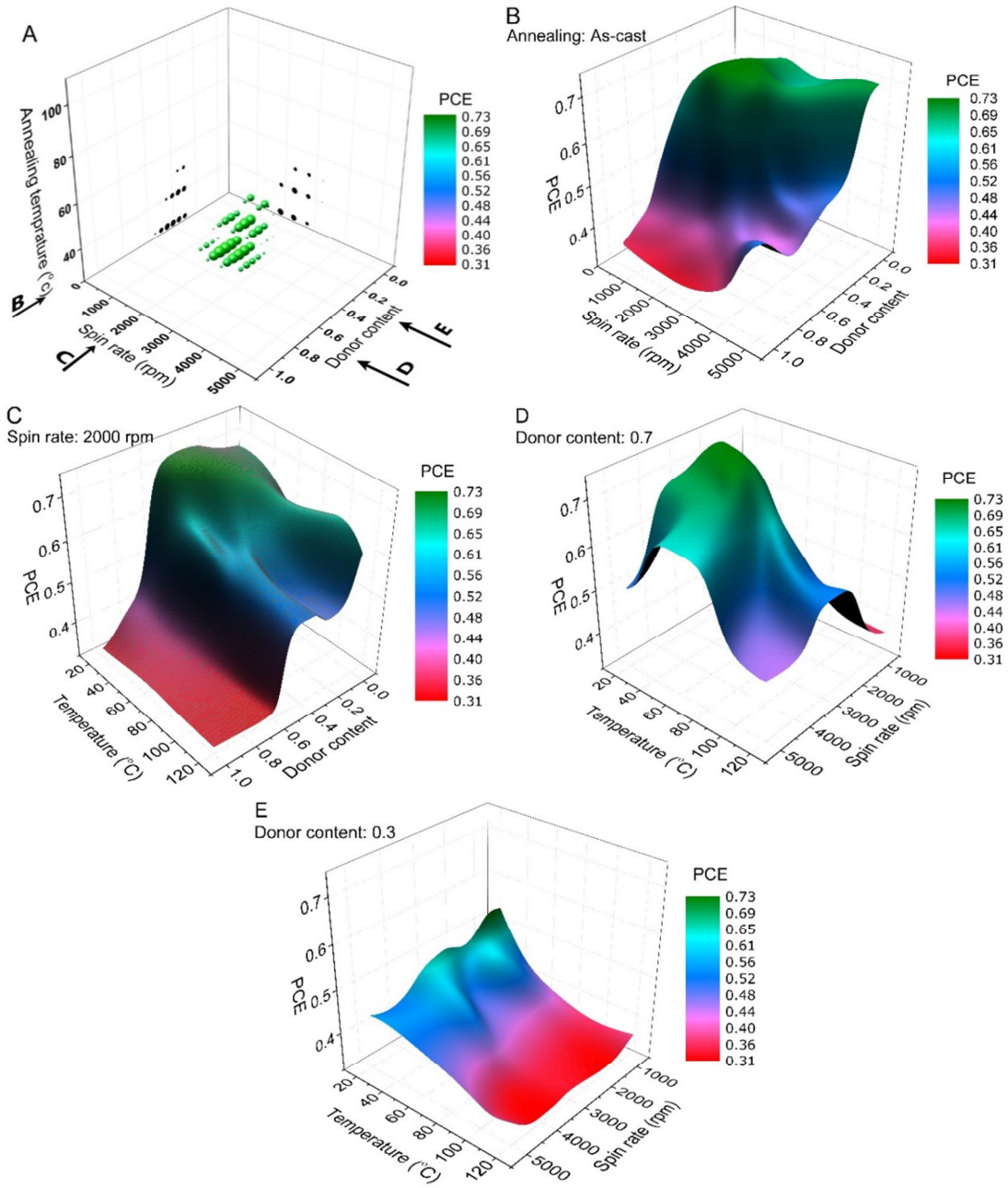

Figure 9: Three-dimensional plots predicted from the ANN model representing the effect of donor content, annealing and spin rate on PCE.

4. Conclusion

The present study was designed to determine the capability of AI technics in modeling the BHJ solar cell casting parameters. In case of successful integration of our suggested ANN/GA hybrid model, it would end in decreasing the number of experiments needed to optimize the BHJs during cell casting practices and delivering brighter deduction of the individual impacts of the input variables on the working parameters.

The model has been constructed on the basis of 27 experimental scenarios by variation of donor content, annealing temperature and film casting spin rate of BHJ cells (each variable in 3 levels) with a single junction BT($TDPP_{EH}TTT_{C6}$)$_2$:$PC_{71}BM$ BHJ. Results showed successful convergence during the training process, and the low difference between the error of training and test steps concedes the capability of the proposed code to learn the trends from the limited number of data without overfitting.

Moreover, the current findings add substantially to our understanding on the impact of cell functionalities and specific variable range to obtain the higher cell working parameters. For the interested DPP-BT based donor molecule,the challenge of modifying PCE is easier at the higher levels of J_{sc}. While the same variation trend was observed for the J_{sc}, and FF value by changing the aforesaid manufacturing parameters, this model declared that the trends of V_{oc} and J_{sc} are in an opposite direction but with a mild sloop. This finding supports the scheme that V_{oc} indirectly depends on bulk characteristics while J_{sc} and FF are closely dependent on the morphology of the active layer and device characteristics. Based on the stated outcomes, this research provides a powerful methodology to help the researchers in the field of organic electronics to learn sufficient data from less experiment. This investigation, as a significant progress, can be considered for many other cell manufacturing variables (such as cell thickness and heating rate during the annealing process) which affect final PCE performance.

5. References

1. C. Dyer-Smith, J. Nelson, Y. Li, Organic solar cells, in: McEvoy's handbook of photovoltaics (Third Edition), Elsevier, 2017, pp. 567-597.
2. B. H. Jørgensen, K. K. Andersen, E. J. Wilson, Accelerating the clean energy revolution - perspectives on innovation challenges: DTU International Energy Report 2018, Technical University of Denmark (DTU), 2018.
3. A. J. Heeger, 25th Anniversary article: bulk heterojunction solar cells: understanding the mechanism of operation, *Adv. Mater.*, 26(2014), 10-28.
4. Q. Wang, Y. Xie, F. Soltani-Kordshuli, M. Eslamian, Progress in emerging solution-processed thin film solar cells–Part I: polymer solar cells, *Renewable Sustainable Energy Rev.*, 56(2016), 347-361.
5. Y. Yang, G. Li, Progress in high-efficient solution process organic photovoltaic devices, Springer, 2016.
6. T. Heumueller, W. R. Mateker, A. Distler, U. F. Fritze, R. Cheacharoen, W. H. Nguyen, M. Biele, M. Salvador, M. von Delius, H. J. Egelhaaf, M.D. McGehee, C.J. Brabec, Morphological and electrical control of fullerene dimerization determines organic photovoltaic stability, *Energy Environ. Sci.*, 9(2016), 247-256.
7. Y. Lin, F. Zhao, Q. He, L. Huo, Y. Wu, T.C. Parker, W. Ma, Y. Sun, C. Wang, D. Zhu, High-Performance Electron Acceptor with Thienyl Side Chains for Organic Photovoltaics, *J. Am. Chem. Soc.*, 138(2016), 4955-4961.
8. S. K. Jha, J. Bilalovic, A. Jha, N. Patel, H. Zhang, Renewable energy: Present research and future scope of Artificial Intelligence, *Renew. Sustain. Energy Rev.*, 77(2017), 297-317.
9. J. D. Perea, S. Langner, M. Salvador, J. Kontos, G. Jarvas, F. Winkler, F. Machui, A. Görling, A. Dallos, T. Ameri, Combined computational approach based on density functional theory and artificial neural networks for predicting the solubility parameters of fullerenes, *J. Phys. Chem. B*, 120(2016), 4431-4438.
10. P. B. Jørgensen, M. Mesta, S. Shil, J.M. García Lastra, K.W. Jacobsen, K.S. Thygesen, M.N. Schmidt, Machine learning-based screening of complex molecules for polymer solar cells, *J. Chem. Phys.*, 148(2018), 241735.
11. A. Aspuru-Guzik, K. Persson, Materials acceleration platform: accelerating advanced energy materials discovery by integrating high-throughput methods and artificial intelligence, mission innovation: innovation challenge 6, 2018.
12. Y. Liu, T. Zhao, W. Ju, S. Shi, Materials discovery and design using machine learning, *J. Materiomics*, 3(2017), 159-177.

13. I. Y. Kanal, G. R. Hutchison, Rapid computational optimization of molecular properties using genetic algorithms: searching across millions of compounds for organic photovoltaic materials, *arXiv preprint arXiv:1707.02949*, (2017).
14. M. Hosseinnezhad, M.R. Saeb, S. Garshasbi, Y. Mohammadi, Realization of manufacturing dye-sensitized solar cells with possible maximum power conversion efficiency and durability, *Sol. Energy*, 149(2017), 314-322.
15. B. Walker, A. Tamayo, D.T. Duong, X.D. Dang, C. Kim, J. Granstrom, T.Q. Nguyen, A systematic approach to solvent selection based on cohesive energy densities in a molecular bulk heterojunction system, *Adv. Energy Mater.*, 1(2011), 221-229.
16. A. Ashtiani Abdi, F. Nourmohammadian, T. Ameri, Energy level gamut, a wide-angle lens to look at photoelectronic properties of Diketopyrrolopyrrole-Benzothiadiazole based small molecules, *Manuscript submitted*, (2018).
17. F. Fernandes, L. Lona, Neural network applications in polymerization processes, *Braz. J. Chem. Eng.*, 22(2005), 401-418.
18. M. R. Saeb, B. Rezaee, A. Shadman, K. Formela, Z. Ahmadi, F. Hemmati, T.S. Kermaniyan, Y. Mohammadi, Controlled grafting of vinylic monomers on polyolefins: a robust mathematical modeling approach, *Des. Monomers Polym.*, 20(2017), 250-268.
19. D. Graupe, Principles of artificial neural networks, World Scientific Publishing, New Jersey, 2013.
20. A. Lipowski, D. Lipowska, Roulette-wheel selection via stochastic acceptance, *Physica A*, 391(2012), 2193-2196.
21. E. J. Hughes, Evolutionary Many-Objective optimisation: many once or one many?, in: 2005 IEEE Congress on Evolutionary Computation, IEEE, Edinburgh, Scotland, 2005, pp. 222-227.
22. K. Deb, Multi-objective optimization using evolutionary algorithms, John Wiley & Sons, 2001.
23. K. Deb, A. Pratap, S. Agarwal, T. Meyarivan, A fast and elitist multiobjective genetic algorithm: NSGA-II, *IEEE Trans. Evolutionary Comput.* 6(2002), 182-197.
24. E. Zitzler, L. Thiele, An evolutionary algorithm for multiobjective optimization: The strength pareto approach, in, Computer Engineering and Networks Laboratory Zurich, 1998.
25. A. Konak, D.W. Coit, A.E. Smith, Multi-objective optimization using genetic algorithms: A tutorial, *Reliab. Eng. Syst. Saf.*, 91(2006), 992-1007.
26. D. Bartesaghi, I. del Carmen Pérez, J. Kniepert, S. Roland, M. Turbiez, D. Neher, L.J.A. Koster, Competition between recombination and extraction of free charges determines the fill factor of organic solar cells, *Nat. Commun.*, 6(2015).
27. B. Ray, M.A. Alam, , Random vs regularized OPV: Limits of performance gain of organic bulk heterojunction solar cells by morphology engineering, *Sol. Energy Mater. Sol. Cells*, 99(2012), 204-212.
28. H. Hoppe, N. Arnold, D. Meissner, N. Sariciftci, Modeling of optical absorption in conjugated polymer/fullerene bulk-heterojunction plastic solar cells, *Thin Solid Films*, 451(2004), 589-592.
29. K. Maturova, S. Van Bavel, M. Wienk, R. Janssen, M. Kemerink, Morphological device model for organic bulk heterojunction solar cells, *Nano Lett.*, 9(2009), 3032-3037.
30. T. Ameri, G. Dennler, C. Waldauf, P. Denk, K. Forberich, M.C. Scharber, C.J. Brabec, K. Hingerl, Realization, characterization, and optical modeling of inverted bulk-heterojunction organic solar cells, *J. Appl. Phys.*, 103(2008), 084506.
31. T. Ameri, G. Dennler, C. Waldauf, H. Azimi, A. Seemann, K. Forberich, J. Hauch, M. Scharber, K. Hingerl, C.J. Brabec, Fabrication, optical modeling, and color characterization of semitransparent bulk-heterojunction organic solar cells in an inverted structure, *Adv. Funct. Mater.*, 20(2010), 1592-1598.
32. L. Koster, E. Smits, V. Mihailetchi, P. Blom, Device model for the operation of polymer/fullerene bulk heterojunction solar cells, *Phys. Rev. B: Condens. Matter*, 72(2005), 085205.
33. B. Watts, W.J. Belcher, L. Thomsen, H. Ade, P.C. Dastoor, A quantitative study of PCBM diffusion during annealing of P3HT: PCBM blend films, *Macromolecules*, 42(2009), 8392-8397.
34. R. Häusermann, E. Knapp, M. Moos, N. Reinke, T. Flatz, B. Ruhstaller, Coupled optoelectronic simulation of organic bulk-heterojunction solar cells: Parameter extraction and sensitivity analysis, *J. Appl. Phys.*, 106(2009), 104507.
35. O. Wodo, S. Tirthapura, S. Chaudhary, B. Ganapathysubramanian, A graph-based formulation for computational characterization of bulk heterojunction morphology, *Org. Electron.*, 13(2012), 1105-1113.
36. Y. J. Kim, Y. R. Cheon, J. Y. Back, Y. H. Kim, D. S. Chung, C. E. Park, Naphtho [2, 1-b: 3, 4-b′] dithiophene-based Bulk Heterojunction Solar Cells: How Molecular Structure Influences Nanoscale Morphology and Photovoltaic Properties, *Chem. Phys. Chem.*, 15(2014), 3626-3633.
37. M. C. Scharber, On the Efficiency Limit of Conjugated Polymer: Fullerene-Based Bulk Heterojunction Solar Cells, *Adv. Mater.*, 28(2016), 1994-2001.
38. M. C. Scharber, D. Mühlbacher, M. Koppe, P. Denk, C. Waldauf, A.J. Heeger, C.J. Brabec, Design rules for donors in bulk-heterojunction solar cells—Towards 10% energy-conversion efficiency, *Adv. Mater.*, 18(2006), 789-794.
39. K. Vandewal, J. Widmer, T. Heumueller, C.J. Brabec, M.D. McGehee, K. Leo, M. Riede, A. Salleo, Increased open ‐ circuit voltage of organic solar cells by reduced donor ‐ acceptor interface area, *Adv. Mater.*, 26(2014), 3839-3843.

40. N. K. Elumalai, A. Uddin, Open circuit voltage of organic solar cells: an in-depth review, *Energy Environ. Sci.*, 9(2016), 391-410.

41. J. C. Blakesley, D. Neher, Relationship between energetic disorder and open-circuit voltage in bulk heterojunction organic solar cells, *Phys. Rev. B: Condens. Matter*, 84(2011), 075210.

How to cite this article:
A. Ashtiani Abdi, F. Nourmohammadian, Y. Mohammadi, M. R. Saeb, Control over Power Conversion Efficiency of BHJ Solar Cells: learn more from less, with artificial intelligence. Prog. Color Colorants Coat., 12 (2019), 1-14.